Deterministic Separation of Cancer Cells from Blood at 10 mL/min

Kevin Loutherback[1,2,4], Joseph D'Silva[1,2], Liyu Liu[1,3], Amy Wu[1,2], Robert H. Austin [1,3] & James C. Sturm [1,2]

[1]*Princeton Institute for the Science and Technology of Materials (PRISM),*

[2]*Department of Electrical Engineering, Princeton University, Princeton, NJ*

[3]*Department of Physics, Princeton University, Princeton, NJ*

[4]*Current Address: Lawrence Berkeley National Laboratory, Berkeley, CA*

Circulating tumor cells (CTCs) and circulating clusters of cancer and stromal cells have been identified in the blood of patients with malignant cancer and can be used as a diagnostic for disease severity, assess the efficacy of different treatment strategies and possibly determine the eventual location of metastatic invasions for possible treatment. There is thus a critical need to isolate, propagate and characterize viable CTCs and clusters of cancer cells with their associated stroma cells. Here, we present a microfluidic device for mL/min flow rate, continuous-flow capture of viable CTCs from blood using deterministic lateral displacement arrays. We show here that a deterministic bump array can be designed such that it will isolate with efficiency greater than 85% CTCs over a large range in sizes from millimeter volume clinical blood samples in minutes, with no effect on cell vitality so that further culturing and analysis of the cells can be carried out.

Much of the recent work in this area has focused on capturing cells on epithelial antibody-coated surfaces in microfluidic flow channels[11,12], but these devices must be operated slowly ($\sim$ mL/hr) to maintain capture efficiency and viable cell recover is difficult because cells are strongly bound to the surface once they attach. Further, it is now clear that circulating clusters of cancer and stromal cells (the latter forming the "seed and soil" hypothesis of metastasis [1–7], in principle single patient analysis would aid in the development personalized treatments[8,9]. Because of the rarity of CTCs (1-1000) cells/mL)[3] compared to other cells in the blood and the large variation in their morphology [10], large volumes have to be processed to deliver a sufficient number for statistical detection and detailed characterization of the heterogeneity. CTCs (diameters 15 - 30 μm) are on average larger than other cells in blood (2 - 15 μm)[13], giving the possibility of enrichment

with a size-based separation technique. Circulating clusters of cancer and stromal cells are even larger, up to 200 μm in diameter [6]. Several methods involving membrane based filtration[14–16] or devices relying on inertial effects[17,18] have been developed to exploit this size difference. Both of these approaches have yielded CTCs from blood with high capture efficiencies and enrichment factors. However, because of the rarity of these cells (1-1000) cells/mL)[3] compared to other cells in the blood (red blood cells - 10^9 cells/mL, platelets - 10^8 cells/mL, and white blood cells - 10^6 cells/mL), large volumes of blood have to be processed to deliver a sufficient number for statistical detection or study, and a large dynamic range of sizes must be accomodated ranging from single cells to cell clusters. Because of the need for a large range of sizes, clogging may be an issue with membrane-based technology, while the throughput of inertial techniques is limited by the heavy dilutions that are necessary to maintain separation resolution.

Deterministic lateral displacement is a microfluidic size-based particle sorting method with excellent size selectivity which does not depend on first order on the rate of flow since it does not rely on diffusion, adaptability to sorting multiple particle sizes[19] , and dynamic control of critical particle sizes[20]. It has been demonstrated under a broad range of operating conditions, sorting particles from 100 nm[21] to 30 um[22]. In the method, an array of microposts direct particles above a critical size at an angle with respect to the fluid flow direction so that the larger particles will eventually become concentrated at one sidewall of the array. Using such an array, large particles can be concentrated from an input stream and harvested at the end of the array by collecting the output fluid stream separate from the rest of the fluid leaving the array. However, it has never been demonstrated that a deterministic lateral displacement array can process the volumes needed for

selection of rare circulating cells in whole blood in times of the order of minutes, and maintained cell viability.

A unique aspect of the deterministic bump array present here is that triangular posts are used rather than cyindical posts. Triangles provide for increased throughput and less clogging compared to circular posts [23] microfluidic and Inglis' wall design is used to ensure flow uniformity near channel walls where particles are concentrated [24]. Triangle posts offer a far greater range of complexity in the motion of objects in a deterministic bump array because of the impact of rotations of the posts in the array on the motion of objects in the array, as shown in Fig. 1 . The ability of the device to direct the motion of particles is shown in the fluorescent trajectories of 3.1 μm polystyrene beads in an array with 12 μm gaps, 18 μm posts, 1/20 array tilt and 2.0 μm critical size. Beads that are uniformly distributed at the array inlet are directed towards the central wall as they travel through the array. At the outlet, nearly all of the beads are concentrated against the wall and collected in the narrow collection output.

The layout of a concentrator device which allows this breakthrough in performance is shown in Fig. 2 . It is composed of a 2.5 mm wide by 25 mm long flow chamber filled with a mirrored array of 58 μm triangular posts with 42 μm gaps between posts. One axis of the array is tilted at an angle of 1/20 radians with respect to the direction of fluid flow, which should give a critical size of 7 microns. According the operating principles of DLD, large particles above a designed critical size (e.g. the cancer cells) will flow along this tilted axis of the array, while the fluid and small particles flow in the horizontal direction defined by the array sidewalls. The top section in the

mirrored array directs large particles downward towards the central wall while the bottom section directs them upward. This allows the device width to be doubled without increasing the array length, which must typically be scaled with the array width as W/ϵ to ensure all large particles are displaced to the central wall. A fluid containing targeted particles is brought in from a single inlet and flowed through the array. While traversing the array, large particles are concentrated towards the center of the flow chamber and collected at a narrow collection output while all other fluid is directed to a waste outlet. Devices are etched into a silicon wafer to a depth of 60 μm and sealed with a PDMS-coated glass cover slide. Three devices are tiled in plane on each silicon layer and external connections are made by mating an acrylic manifold to through-wafer holes etched into device at inlet and outlet ports. The manifold is spring-loaded to withstand applied pressures up to 4.7 atmospheres without leaking. Manifold, devices, and tubing are first wet with a running buffer of 1x PBS, 1% BSA, and 1 mM EDTA. 5 mL of fluid was processed in each experiment at various flow rates that were controlled by a syringe pump. The pressure drop across the device was measured at 4 atmospheres at 10 mL/min flow rate for buffer and scaled linearly with flow rate.

Experiments were performed with approximately 10^7 cancer cells from breast or prostate cell lines in 1 mL of growth medium spiked into buffer or blood diluted with buffer. Cells are cultured using standard methods and used immediately after passage. Premalignant (MCF10A) and malignant (MDAMB231) epithelial breast cells contained a GFP or RFP construct that allowed them to be easily differentiated from other non-fluorescent cells in solution. Device functionality with cancer cells was confirmed by observing the trajectories of MDAMB231 breast cells expressing GFP with epifluorescent microscopy at a flow rate of 100 $\mu L/min$ (Fig. 3). Using cells in buffer,

we can clearly see that cells enter the device broadly distributed from a single inlet as they enter the array and are focused against the central wall and directed into the collection output at the end of the array.

We confirmed the function of the DLD array at high flow rate by processing MCF10A breast cells spiked in the wetting solution at 10 mL/min. 1 mL of growth medium with $\sim 10^7$ cells was diluted to 10 mL with the wetting solution and 5 mL of sample was processed in 30 s. Concentrations and size distribution of cells were measured for input, collection, and waste solutions using a Coulter counter. From an initial concentration of 3.75 x 10^6cells/mL with average size $19.5\,\mu m$, the collection output had a concentration of 2.1 x 10^7 cells/mL with average size $19.5\,\mu m$ while waste output had a concentration of 3.7 x 10^5 cells/mL with average size $19.0\ \mu m$. Factoring in the volume of each output (V_c = 0.8 mL, V_w = 4.2 mL), we can calculate the capture efficiency as the ratio of cells in the collection output to the total number of cells in both outputs $\frac{\#\ collected\ cells}{total\ cells} = \frac{C_c V_c}{C_c V_c + C_w V_w}$. Using this definition, 91% of the targeted cells were collected by the device.

Experiments were then performed with cancer cells spiked into blood to assess the potential for separating CTCs from blood. Blood was supplied by donors from the Interstate Blood Bank (Memphis, TN), shipped overnight and used within one day. Since blood has a higher viscosity than water, a dilution between 5 and 20 times was performed to ensure that the device operated below the pressure ceiling. In a first experiment, 500 μL of blood was added to 1 mL of growth medium with $\sim 10^7$ malignant MDAMB231 breast cells and then diluted to a total volume of 10

mL with the wetting solution. 5 mL of this mixture was processed at 10 ml/min flow rate and the output solutions were analyzed with a flow cytometer. MDAMB231 cells used expressed a red fluorescent protein dTomato that was used to distinguish them from other cells in the mixture which had no fluorescence. 50,000 total cells were analyzed from the input, collection output and waste output. In each run and the number of large, fluorescent cells were enumerated from multivariable analysis. 4.9% of the input cells were cancer cells, while 16.7% of collection output cells and 0.6% of waste output cells were cancer cells. If we assume that the concentrations of other cells remain constant, we can normalize these percentages to the ratio of cancer cells to other cells in each solution and get 0.05, 0.2 and 0.006 for input, collection and waste solutions respectively and a capture efficiency in these conditions of 86%.

For 10 mL/min flow rate, the fluid velocities in the device range from near zero at the post edges to $\sim$ 1.5 m/s in the middle of a gap between posts. This subjects the cells to an high shear stress that might damage them. The strength of shear forces in a flow are characterized by a shear rate defined as $\partial v_x/\partial y$, where x is the flow direction and y is the direction across a gap. The typical range of shear rates in the body is 10 to 10^3 s^{-1} [25]. Cell viability was measured by application of 0.4%w Trypan blue in saline at a 10:1 dilution to input and output samples, vortexing, incubating for 5 min at room temperature, and examining the resulting solution with a haemocytometer.

Passing through the DLD array had no effect on cell viability in several different cell lines suspended in the running solution across a wide range of flow rates. In experiments, summarized in Table 1 with three epithelial cell lines (MDAMB231, PC3, MCF10A) at various flow rates from

0.1 to 10 mL/min, greater than 95% of the cells survived in each experiment. PC3 are malignant prostate cancer cells. While the shear rates in these devices greatly surpasses physiological levels (1-2000 s^{-1} [26], we speculate that the reduced exposure time at the higher flow rates limits cellular damage. At 10 mL/min, cells traverse the entire 25 mm array in about 70 ms. This observation matches with observations of white blood cells in a rotary pump that suggest shear-induced damage is an integral effect over time [27]. That is, cell vitality decreases the longer cells are exposed to high shear. Experiments done by Di Carlo *et al.*[28] to examine gene expression in cells exposed to high shear showed no significant changes. As a result, we do not expect shear-induced cell death or alteration to be a significant limitation in the operation of these devices.

We further assessed cell vitality by culturing cells after they had passed through a device. Approximately 10^6 MDAMB231 cells were spiked into whole blood diluted 10:1 and 5 mL of this solution was driven through a single layer device at 5 mL/min. Red blood cells in the output from the collection channel were lysed with 1x RBC lysis buffer (eBiosciences), washed with the running solution and 500 μL of the resulting solution was placed into a 25 cm^2 culture flask with 3 mL of growth media. Shown in Fig. 4 , the red fluorescent MDAMB231 cells attach to the surface and proliferate. While there is a small background of white blood cells and unlysed red blood cells, the cancer cells seem unaffected.

The 10 mL/min flow rates presented constitute a 50-fold improvement in flow rate over the herringbone-CTC chip used by Stott *et al.*[12], a 10^5-fold improvement over the 10s of $\mu L/min$ historical flow rates in DLD arrays [22,29] and a 100-fold improvement over more recent efforts by Inglis

et al. [30] and are the fastest reported operation of these devices. With internal velocities exceeding 1 m/s and Reynolds number Re $>$ 40, we confirm that the size-based separation functionality is preserved even outside the low Reynolds number flow regime.

In summary, these experiments showed that high efficiency capture of cancer cells from blood is possible at flow rates of 10 ml/m with no effect on cell vitality by using deterministic lateral displacement arrays at flow rates much higher than used in previous microfluidic devices. Operating devices in parallel could easily enable flow rates an order of magnitude larger, and design of more complex heterogenous triangle arrays will allow the separation of a vast range of object sizes with no clogging issues. These results open up the possibility of rapid collection of viable circulating tumor cells and clusters of cancer and stromal cells from the blood of patients with metastatic disease. Capturing and propagating viable cells from patients could allow *in vitro* chemotherapeutic treatments to be studied in vitro to determine which may be the most effective in vivo and allow better study of the development of drug resistance.

1. Nagrath, S. *et al.* Isolation of rare circulating tumour cells in cancer patients by microchip technology. *Nature* **450**, 1235–1239 (2007).

2. Stott, S. *et al.* Isolation of circulating tumor cells using a microvortex-generating herringbone-chip. *Proceedings of the National Academy of Sciences* **107**, 18392 (2010).

3. Langley, R. R. & Fidler, I. J. The seed and soil hypothesis revisited-the role of tumor-stroma interactions in metastasis to different organs. *International Journal of Cancer* **128**, 2527–2535

(2011).

4. Liotta, L. A., Kleinerman, J. & Saidel, G. M. Significance of hematogenous tumor-cell clumps in metastatic process. *Cancer Research* **36**, 889–894 (1976).

5. Cristofanilli, M. *et al.* Circulating tumor cells, disease progression, and survival in metastatic breast cancer. *New England Journal of Medicine* **351**, 781–791 (2004).

6. Al-Mehdi, A. B. *et al.* Intravascular origin of metastasis from the proliferation of endothelium-attached tumor cells: a new model for metastasis. *Nature Medicine* **6**, 100–102 (2000).

7. Maheswaran, S. & Haber, D. Circulating tumor cells: a window into cancer biology and metastasis. *Current opinion in genetics & development* **20**, 96–99 (2010).

8. Duda, D. G. *et al.* Malignant cells facilitate lung metastasis by bringing their own soil. *Proceedings of the National Academy of Sciences of the United States of America* **107**, 21677–21682 (2010).

9. Lalmahomed, Z. *et al.* Circulating tumor cells and sample size: the more, the better. *Journal of Clinical Oncology* **28**, e288 (2010).

10. Riethdorf, S. & Pantel, K. Advancing personalized cancer therapy by detection and characterization of circulating carcinoma cells. *Annals of the New York Academy of Sciences* **1210**, 66–77 (2010).

11. Morgan, S. C. & Parker, C. C. Local treatment of metastatic cancer-killing the seed or disturbing the soil? *Nature Reviews Clinical Oncology* **8**, 504–506 (2011).

12. Marrinucci, D. *et al.* Case study of the morphologic variation of circulating tumor cells. *Human Pathology* **38**, 514–519 (2007).

13. Meng, S. *et al.* Circulating tumor cells in patients with breast cancer dormancy. *Clinical cancer research* **10**, 8152 (2004).

14. Lin, H. *et al.* Portable filter-based microdevice for detection and characterization of circulating tumor cells. *Clinical Cancer Research* **16**, 5011 (2010).

15. Vona, G. *et al.* Isolation by size of epithelial tumor cells: A new method for the immunomorphological and molecularcharacterization of circulating tumor cells. *American Journal of Pathology* **156**, 57 (2000).

16. Zheng, S. *et al.* Membrane microfilter device for selective capture, electrolysis and genomic analysis of human circulating tumor cells. *Journal of Chromatography A* **1162**, 154–161 (2007).

17. Bhagat, A., Hou, H., Li, L., Lim, C. & Han, J. Pinched flow coupled shear-modulated inertial microfluidics for high-throughput rare blood cell separation. *Lab Chip* (2011).

18. Hur, S., Mach, A. & Di Carlo, D. High-throughput size-based rare cell enrichment using microscale vortices. *Biomicrofluidics* **5**, 022206 (2011).

19. Huang, L., Cox, E., Austin, R. & Sturm, J. Continuous particle separation through deterministic lateral displacement. *Science* **304**, 987 (2004).

20. Beech, J. & Tegenfeldt, J. Tuneable separation in elastomeric microfluidics devices. *Lab Chip* **8**, 657–659 (2008).

21. Morton, K., Sturm, J., Austin, R. & Chou, S. Nanoimprinted fluidic device for continuous separation of nanoparticles. *Proc of μ TAS* **1**, 1014–1016 (2006).

22. Davis, J. *et al.* Deterministic hydrodynamics: Taking blood apart. *Proceedings of the National Academy of Sciences* **103**, 14779 (2006).

23. Loutherback, K. *et al.* Improved performance of deterministic lateral displacement arrays with triangular posts. *Microfluidics and nanofluidics* 1–7 (2010).

24. Inglis, D. Efficient microfluidic particle separation arrays. *Applied Physics Letters* **94**, 013510 (2009).

25. Dintenfass, L. *Blood microrheology: viscosity factors in blood flow, ischaemia, and thrombosis: an introduction to molecular and clinical haemorheology* (Appleton-Century-Crofts, 1971).

26. Freitas, R. *Nanomedicine, volume I: Basic capabilities* (Landes Bioscience Georgetown, TX, 1999).

27. Takami, Y., Yamane, S., Makinouchi, K., Glueck, J. & Nosé, Y. Mechanical white blood cell damage in rotary blood pumps. *Artificial organs* **21**, 138–142 (1997).

28. Hur, S., Henderson-MacLennan, N., McCabe, E. & Di Carlo, D. Deformability-based cell classification and enrichment using inertial microfluidics. *Lab Chip* (2011).

29. Huang, R. *et al.* A microfluidics approach for the isolation of nucleated red blood cells (nrbcs) from the peripheral blood of pregnant women. *Prenatal diagnosis* **28**, 892–899 (2008).

30. Inglis, D., Lord, M. & Nordon, R. Scaling deterministic lateral displacement arrays for high throughput and dilution-free enrichment of leukocytes. *Journal of Micromechanics and Microengineering* **21**, 054024 (2011).

Flow Rate (mL/min)	Cell Type	Viability	Cells Counted	V_{max} (cm/s)	Shear Rate (s^{-1})	Transit Time (s)
0.1	MDAMB231	0.95	61	1.5	750	7.0
0.1	PC3	0.96	28	1.5	750	7.0
0.5	MCF10A	0.96	51	7.5	3750	1.4
5.0	MCF10A	1.00	123	75	37500	0.14
10.0	MCF10A	0.99	125	150	75000	0.07

Table 1: **Viability Experiment Summary.** V_{max} defined as maximum velocity across a gap extracted from numerical simulation, shear rate $\partial v_x/\partial y$ estimated as maximum velocity in the gap divided by half the 42 μm gap. Array length is 25 mm.

Figure 1 Anisotropic Conduction Schematic of the movement of 3 different cells in a deterministic lateral displacement array consisting of triangular posts. In a properly designed array, cells below a lowest average hydrodynamic size, such as red blood cells and white blood cells, simply follow the hydrodynamic streamlines. Cells above a critical size, such as circulating tumor cells and circulating clumps, are pushed by the posts into adjacent streamlines and move diagonally to the flow.

Figure 2 High Throughput Device. A concentrator deterministic lateral displacement array with one input and two outputs (collection and waste) is used. Fluorescent micrographs of the trajectories of 3.1 μm beads in arrays with 12 μm gaps, 18 μm triangular posts, 1/20 array tilt and 2.0 μm critical size highlight device function. Using a mirrored design, large particles dispersed in the inlet are focused against the central channel wall, where they can be collected at the narrow collection output while other particles enter the waste outlet.

Figure 3 CTC enrichment in DLD array. Trajectories of GFP-expressing MDAMB231 breast cells in an array with 42 μm gaps, 1/20 array tilt, and 7 μm critical particle size at device inlet and outlet at flow rate of 500 $\mu L/min$. Cells are evenly dispersed at inlet but are concentrated against central wall at outlet and directed to narrow collection outlet.

Figure 4 MDAMB231 cells are unaffected by passage through the DLD array. Time series of cancer cells (red) spiked in blood shows proliferation in a culture flask after flow through device at 5 mL/min flow rate.

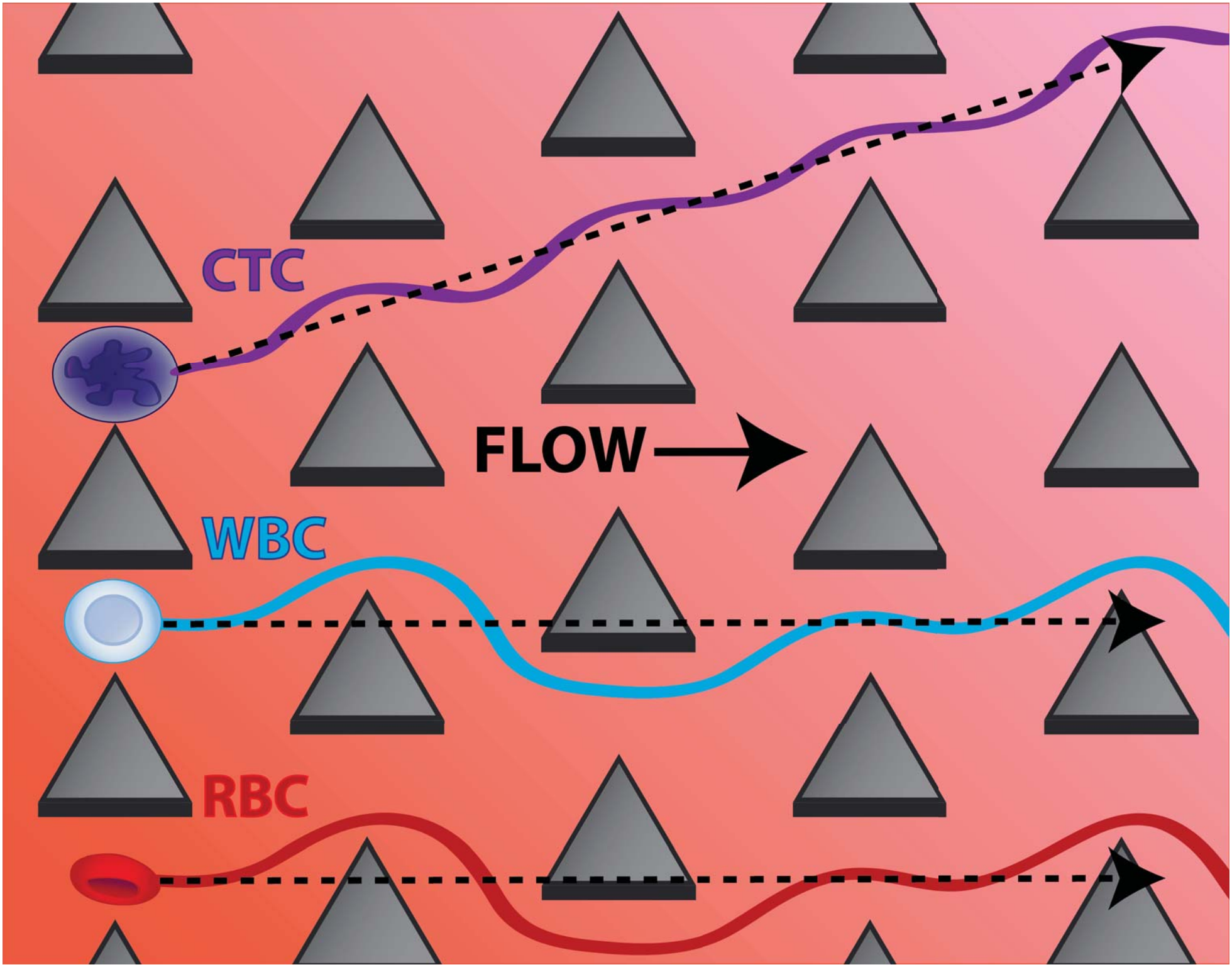

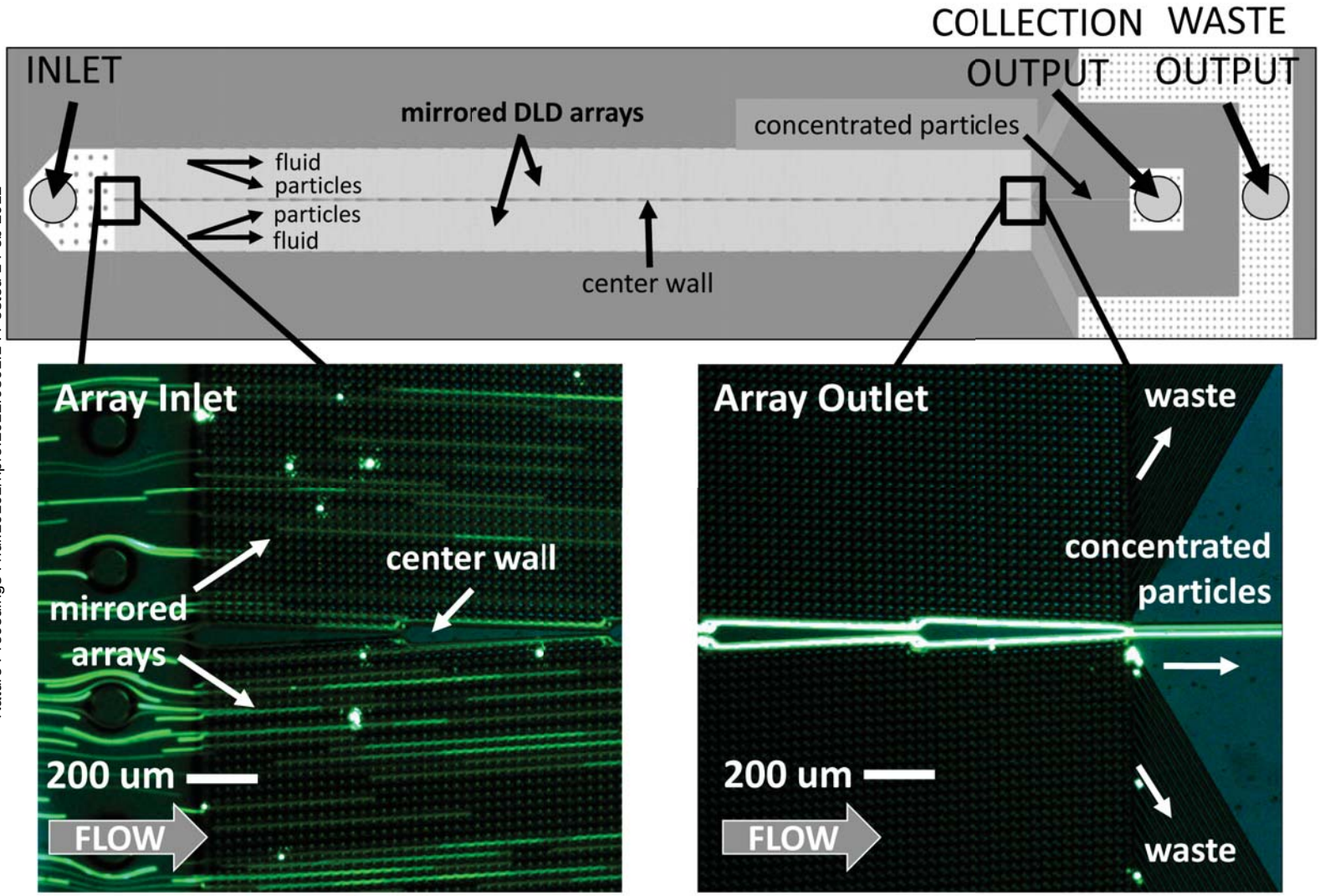

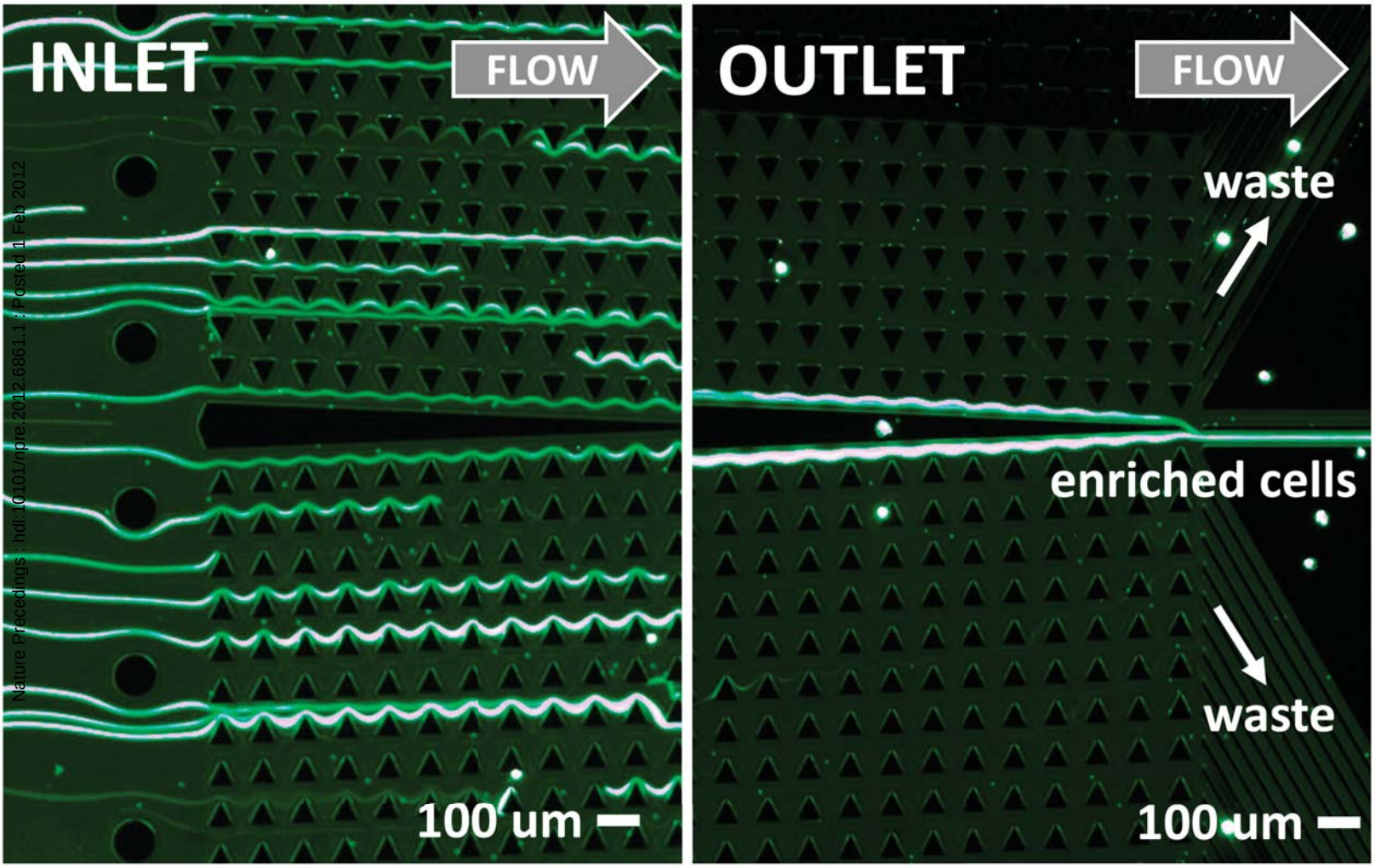

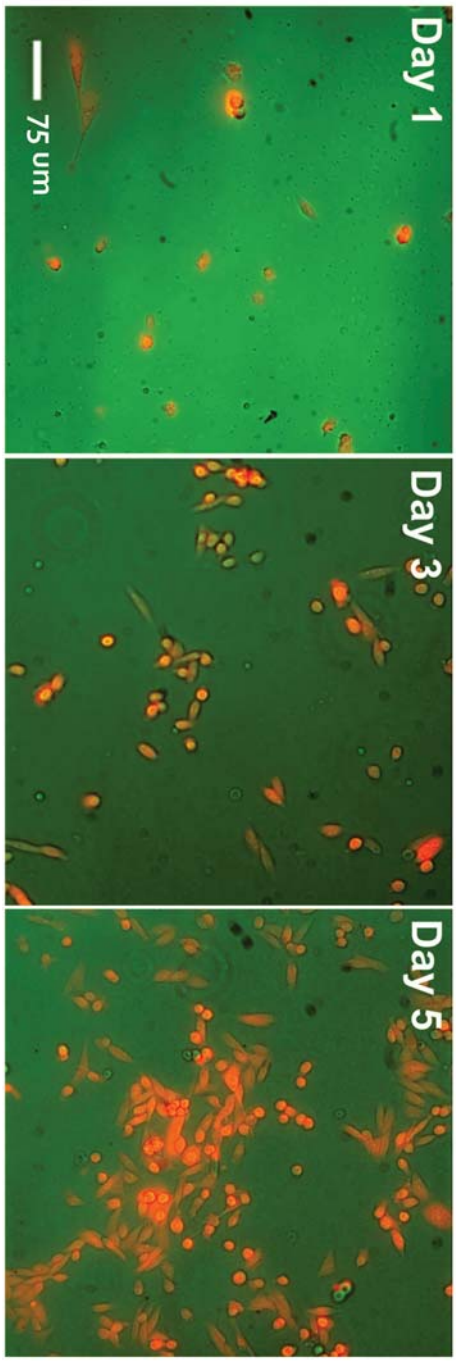
Day 1
75 um
Day 3
Day 5